Boletim da Sociedade Astronômica Brasileira, **35**, no. 1, 145-149

Optical mass proxies for galaxy clusters from probabilistic memberships

L. Doubrawa[1], E. S. Cypriano[1], A. Finoguenov[2], P. A. A. Lopes[3], M. Maturi[4,5], A. H. Gonzalez[6], & R. Dupke[7,8,9]

[1] Instituto de Astronomia, Geofísica e Ciências Atmosféricas, Universidade de São Paulo, Rua do Matão 1226, 05508-090 São Paulo, Brazil e-mail: lia.doubrawa@usp.br
[2] Department of Physics, University of Helsinki, P.O. Box 64, FI-00014 Helsinki, Finland
[3] Observatório do Valongo, Universidade Federal do Rio de Janeiro, Ladeira do Pedro Antônio 43, Rio de Janeiro RJ 20080-090, Brazil
[4] Zentrum für Astronomie, Universitatät Heidelberg, Philosophenweg 12, D-69120 Heidelberg, Germany
[5] Institute for Theoretical Physics, Philosophenweg 16, D-69120 Heidelberg, Germany
[6] Department of Astronomy, University of Florida, Gainesville, FL 32611-2055, USA
[7] Observatório Nacional, Rua General José Cristino, 77, São Cristóvão, 20921-400, Rio de Janeiro, RJ, Brazil
[8] Department of Astronomy, University of Michigan, 311 West Hall, 1085 South University Ave., Ann Arbor, USA
[9] Department of Physics and Astronomy, University of Alabama, Box 870324, Tuscaloosa, AL, USA

Abstract. Accurate galaxy cluster mass estimates play a crucial role in refining cosmological parameters through count analyses. Therefore, it is essential to identify reliable tracers that exhibit minimal intrinsic scatter and can be readily deduced from observations. In this work, we explore the photometric information to create mass proxies using a simulated dataset. For this, we use AME, an adaptive membership estimator that makes minimal assumptions about the galaxy cluster's properties. With the membership assignments, we derive richness, total stellar mass, and optical luminosity. Our sample is composed of 919 galaxy clusters within the redshift range of $0.05 < z < 0.45$, and masses ranging from $12.8 < \log_{10}(M/M_\odot) < 15$. Richness estimates present an offset from the mock known values of -0.01 ± 0.12. The scaling relations show a scatter of $\sigma_{log_{10}(M|\lambda)} = 0.181 \pm 0.009$ dex for richness, $\sigma_{log_{10}(M|M^\star_\lambda)} = 0.097 \pm 0.005$ dex for stellar mass, and $\sigma_{log_{10}(M|L_\lambda)} = 0.151 \pm 0.007$ dex for optical luminosity. We also discuss the impact of small displacements in the cluster center and redshift. We conclude that our algorithm provides competitive cluster mass proxies with low scatter for photometric surveys.

Resumo. Estimativas precisas de massa de aglomerados de galáxias desempenham um papel crucial na melhoria dos parâmetros cosmológicos por meio de análises de contagem. Portanto, é essencial identificar traçadores confiáveis que apresentem dispersão intrínseca mínima e possam ser facilmente deduzidos a partir de observações. Neste trabalho, exploramos as informações fotométricas para criar estimadores de massa usando um conjunto de dados simulado. Para isso, utilizamos o AME, um estimador de probabilidades de pertencimento das galáxias que faz suposições mínimas sobre as propriedades do aglomerado de galáxias. Com as atribuições de probabilidades, obtemos riqueza, massa estelar total e luminosidade óptica. Nossa amostra é composta por 919 aglomerados de galáxias dentro da faixa de redshift de $0.05 < z < 0.45$, e massas variando de $12.8 < \log_{10}(M/M_\odot) < 15$. As estimativas de riqueza apresentam um deslocamento dos valores simulados conhecidos de -0.01 ± 0.12. As relações de escala mostram uma dispersão de $\sigma_{log_{10}(M|\lambda)} = 0.181 \pm 0.009$ dex para riqueza, $\sigma_{log_{10}(M|M^\star_\lambda)} = 0.097 \pm 0.005$ dex para massa estelar, e $\sigma_{log_{10}(M|L_\lambda)} = 0.151 \pm 0.007$ dex para luminosidade óptica. Também discutimos o impacto de pequenos deslocamentos de centralização e redshift dos aglomerados. Concluímos que nosso algoritmo fornece estimadores de massa competitivos e de baixa dispersão para levantamentos fotométricos.

Keywords. Galaxies: clusters: general – Galaxies: groups: general – Methods: statistical

1. Introduction

Cosmological surveys like KiDS (de Jong et al. 2013), DES (The Dark Energy Survey Collaboration 2005), WISE (Wright et al. 2010), and others, provide vast datasets with billions of galaxies. Analyzing these data enhances our understanding of the Universe's large-scale structure and evolution. Galaxy clusters, as tracers of overdensity peaks in matter distribution, offer a sensitive indicator of cosmic density and clustering evolution. Consequently, they serve as powerful tools for constraining cosmological parameters (e.g. Reiprich & Böhringer 2002; Vikhlinin et al. 2009; Pacaud et al. 2016; Ider Chitham et al. 2020; Finoguenov et al. 2020). However, this approach relies on precise mass estimates for the detected systems. As direct observation cannot provide these estimates, we must depend on observable proxies for halo masses.

An ideal mass proxy should show limited dependence on the cluster's dynamical state, exhibit minimal intrinsic scatter, and be easily accessed.

In recent decades, researchers have explored various independent mass proxies to minimize uncertainties and systematic effects. Statistical uncertainties can be reduced to approximately 0.2-0.3 dex for parameters such as cluster optical richness (Lopes et al. 2009), temperature, X-ray luminosity (Sereno et al. 2019), stellar mass (Pereira et al. 2018), and Sunyaev-Zel'dovich effect signal (Pratt & Bregman 2020). However, statistics for low-mass systems such as galaxy groups remain limited and need further investigation.

Imaging surveys utilizing narrow-band filters hold particular significance in the galaxy cluster studies. These surveys serve as an intermediary between broad-band imaging and spectroscopic surveys, offering enhanced precision and accuracy for the galaxies' photometric redshifts (photo-z's). Notable examples include J-PAS (Benitez et al. 2014), S-PLUS (Mendes de Oliveira et al. 2019), and J-PLUS (Cenarro et al. 2019). Regarding group and cluster detections, this transition also affects cluster finder algorithms. Methodologies are evolving from color-based approaches to those capable of leveraging increased photometric

information, as seen in the performance and algorithm selection discussed in Euclid Collaboration et al. (2019).

Hence, it is necessary to reassess membership estimation strategies and techniques to derive mass proxies with minimal scatter utilizing photometric data. However, a challenge in dealing with photo-z is the scale of the redshift uncertainties. A typical error of 0.01 in photo-zs translates to 3000 km/s, surpassing the typical virialized cluster velocity dispersion estimated with spectroscopic redshifts by 3-6 times. This discrepancy results in contamination by line-of-sight galaxies and may generate false cluster detections by connecting unrelated structures (Weinberg et al. 2013).

This issue of galaxy membership for groups and clusters has been engaged in recent studies by Castignani & Benoist (2016); Bellagamba et al. (2019); Lopes & Ribeiro (2020). The authors discuss the use of a continuous probabilistic membership, as opposed to binomial ones, which can provide a better description of the data. Thus, this approach enables the establishment of various galaxy-based mass proxies, which are determined by assigning weights to galaxy properties based on their membership probabilities, such as luminosity, stellar masses, or other relevant factors.

Inspired by the emergence of ongoing and upcoming wide photometric surveys, we conduct an analysis of the distributions of galaxy groups/clusters down to $\log_{10}(M) > 12.8$ $M_\odot$ based on a sky simulation of the Southern Photometric Local Universe Survey (S-PLUS, Mendes de Oliveira et al. 2019) up to redshift $z = 0.45$. Employing AME, an adaptive membership algorithm (Doubrawa et al. 2023), we explore mass proxies such as richness, optical luminosity, and stellar mass derived from these memberships. The significance of richness is discussed by comparing it with the expected value from the simulation. We present scaling relations obtained with the mass proxies, discuss intrinsic scatter, and introduce small offsets to simulate real-case displacements in cluster detection, evaluating their impact on our results. This work relies on the results presented in Doubrawa et al. (2023).

2. Data

To assess the effectiveness of our estimator, we employ a simulated sky lightcone catalog created by Araya-Araya et al. (2021); Werner et al. (2022), designed to mimic the characteristics of the S-PLUS survey (Mendes de Oliveira et al. 2019), particularly the features of its initial data release. S-PLUS is a photometric survey of the Southern Sky utilizing 12 optical bands (5 broad and 7 narrow) from a 0.8m telescope situated at Chile/CTIO.

This simulated catalog covers an area of 324 square degrees and is generated using synthetic galaxies based on the analytical model (SAM) by Henriques et al. (2015). The algorithm employs the Millennium simulation (Springel et al. 2005) as a foundation, scaling the equivalent matter density field according to the Planck Collaboration et al. (2014) cosmological framework. The simulation uses a mass resolution of $m_p = 9.6 \times 10^8$ M⊙/h, with only those halos having a corresponding stellar mass greater than 10^8 M⊙/h being considered.

We select all dominant dark matter halos with $M_{c,200} \geq 10^{12.8}$ $M_\odot$. To ensure robust statistical significance, only halos with at least 3 associated galaxies are considered. The associated galaxy members, hereafter referred to as "true members", are identified through the merger history of the system. Galaxies residing in a dark matter halo and evolving into a chosen cluster receive a cluster identification ID, labeled as "haloId." This ID enables easy identification of all galaxies belonging to a specific cluster. The median value of the distribution of member galaxies gives the halos sky positions.

Restricting the catalog to $z < 0.45$, we identify 238 groups with masses ranging from $10^{12.8}$ to $10^{13.5}$ $M_\odot$, 358 clusters with masses between $10^{13.5}$ and 10^{14} $M_\odot$, 249 with masses from 10^{14} to $10^{14.5}$ $M_\odot$, and 76 massive clusters with $M > 10^{14.5}$ $M_\odot$.

To obtain the photometric redshifts, the true values are shifted by a random number from a normal distribution. Here, the standard deviation $\sigma_{MAD,z}$ represents the normalized median absolute deviation, calculated from the comparison between spectroscopic and photometric redshifts for galaxies with a specific magnitude r. The deviations are derived from Molino et al. (2020) for the DR1/S-PLUS survey.

A comparable method is employed to generate the photo-z probability density function (PDF) for each galaxy. However, in these cases, the normal distribution is centered on the generated photometric redshift. This technique takes into account the correlation between the photometric errors and the galaxy's magnitudes.

3. Methods

In this section, we outline the key steps of the adaptive membership estimator (AME, Doubrawa et al. 2023). The algorithm utilizes galaxy catalog projected positions, photo-z probability density functions (PDFs), and cluster coordinates in 2+1D space (zcl, RAcl, and $\mathrm{Dec_{cl}}$) as inputs. To replicate the obtained values in the S-PLUS survey, we describe the photo-z PDFs as Gaussian distributions centered on the photometric redshift.

1. **Remove Non-Members:** Exclude galaxies beyond a 2.5 Mpc radius, and with $|z_{phot,i} - z_{cl}| > 3\sigma_{MAD,z}(1 + z_{cl})$.
2. **Density Profile Calculation:** Compute the galaxy density profile, defining a core radius (R_c) as the break or "knee" in this profile.
3. **Random Redshift Assignment:** Assign a redshift value based on the photo-z PDF for each galaxy within R_c.
4. **Cluster Velocity Dispersion:** Estimate the cluster velocity dispersion using the random redshifts. Apply a 3σ clipping process to remove possible contamination.
5. **HDBSCAN Clustering:** Apply HDBSCAN (Campello et al. 2014) to the remaining galaxies. If more than one clustering is detected, consider the primary counterpart the one with the most galaxies.
6. **Iterative Process:** Repeat steps 3-5 N times. The membership probability for each galaxy is calculated as the ratio of the number of times the galaxy is identified as a member by HDBSCAN to the total number of repetitions: $P_{mem} = N_{mem}/N$.

In step (i), our goal is to prevent the exclusion of galaxies with reasonable chances of being gravitationally bound members from the potential member pool while also minimizing computational costs.

For step (ii), we define a projected aperture, denoted as R_c, based on the radial distribution of galaxies. This profile is computed within an annulus, progressing from the center outward. Overlapping steps of 10 kpc are used, with a log-scaling width ranging from 50–200 kpc. In estimating areas, we rigorously account for survey boundaries using the Monte Carlo method, which proves effective in handling potential masked survey areas.

This step is characterized by the identification of a discontinuity in the density gradient, typically occurring during the transition from a cluster-dominated to a field-dominated region.

The abrupt density drop, or "break", often represents a factor of 2 within the chosen steps (in a log10 scale). To pinpoint this break, we employ the Kneedle algorithm (Satopaa et al. 2011). In essence, the algorithm identifies a local minimum by assessing the difference between the density profile and a straight line connecting its initial and final points. The first detected local minimum, is designated as R_c. Galaxies beyond this radius are excluded.

Systematic tests involving different binning and steps were conducted. While larger steps may introduce a positive offset of 30 to 60 kpc across the entire range of radii, refining the binning scheme doesn't significantly bias the results.

In steps (iii) and (iv), we depart from using a point estimation for redshift and instead utilize the entire photo-z PDF. We can reproduce the realization of a redshift measurement by drawing a random value based on the PDF for each galaxy in the remaining sample.

Even after the clippings, some sample contamination is expected. Tests with true member galaxies alone yielded a similar velocity dispersion value, indicating that an interactive approach relating a mock quantity (e.g., richness) to expected velocity dispersion wouldn't significantly improve results. A more stringent cut (1σ) might address this issue for well-behaved PDFs where the limit is smaller than the redshift uncertainty. However, for a more realistic distribution, this approach risks eliminating valuable information. Despite these challenges, applying a 3σ clipping can still provide precise results, as presented below.

Finally, in step (v), we apply the Hierarchical Density-Based Spatial Clustering of Applications with Noise (HDBSCAN) algorithm, which connects points based on proximity and identifies more isolated ones as interlopers.

The membership probability is determined by running the described procedure 100 times ($N = 100$) and calculating the probability for each galaxy based on the number of times it is selected by HDBSCAN over the total trials. This iterative approach leverages multiple redshift realizations from the photo-z's PDFs, maximizing its utilization.

4. Results

4.1. Quantifying the richness accuracy

The primary objective of this study is to establish a methodology capable of generating an optical mass proxy based on photometric information with minimal scatter. Furthermore, our aim is to develop a method applicable across diverse cluster catalogs, spanning from groups to galaxy clusters, without relying on robust modeling assumptions. In utilizing optical richness as a proxy for scaling relations, precision in quantifying richness is essential.

As we have access to the true richness of the sample, we compare the average values provided by the mock with the richness calculated by AME (λ_{AME}). True richness (λ_{True}) is defined as the number of galaxies identified as members by the simulations within R_c from the cluster center. Figure 1 illustrates the agreement between both quantities, with a black dotted line indicating the one-to-one line. Each bin includes a minimum of 10 clusters and/or groups. The residual value between λ_{True} and λ_{AME} is a low and unbiased -0.011 ± 0.119, affirming the quality of our richness estimate.

4.2. Mass proxies scaling relations

The primary challenge in utilizing galaxy clusters for cosmological studies lies in measuring their individual masses. A common approach is to establish correlations between mass and other observable properties, such as optical richness, X-ray luminosity, or total stellar mass. Typically, these relationships are calibrated using a limited sample of objects and then extrapolated to the entire catalog. Lensing surveys, for instance, consider the entire sample in stacked analyses. An effective mass proxy should exhibit minimal intrinsic scatter to yield reliable mass estimates.

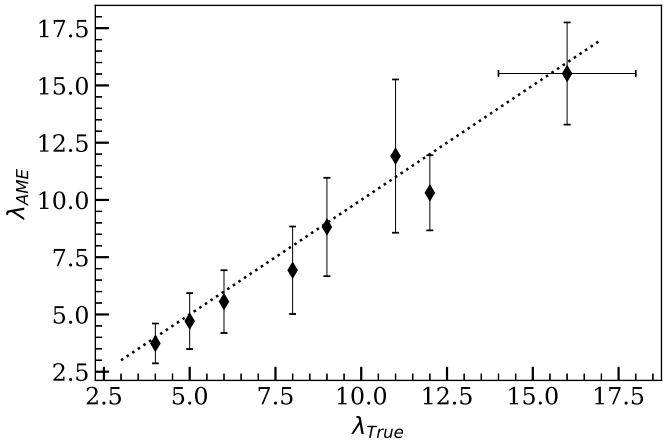

Figure 1. Comparison of richness calculated with the adaptive membership estimator (λ_{AME}) and the true richness provided by the mock (λ_{True}). Each bin of true richness includes a minimum of 10 clusters. The black dotted line represents the one-to-one relation.

As AME provides the probability of each galaxy being gravitationally bound to a specific cluster, we can leverage this capability to characterize the cluster sample by computing various properties, weighted by membership probabilities. For instance, using magnitude information in the r-band, we can estimate the structure total optical luminosity by summing up the contribution of each galaxy luminosity multiplied by its membership, such as $L_\lambda = \sum L_i P_i = \sum 10^{0.4[4.42-M_i]} P_i$. Here, the solar absolute magnitude in the r-band is denoted by 4.65 ($SDSS_r$, Willmer 2018), and M_i represents the absolute magnitude of the i-th galaxy in the same band. Similarly, the stellar mass of mock galaxies can be utilized to derive the structure's total stellar mass by employing a comparable procedure: $M^\star_\lambda = \sum M^\star_i P_i$, with $M^\star_i$ as the stellar mass of the i-th galaxy.

To derive the mock quantities we apply the same concept, where P_i is one for a true member galaxy and zero otherwise.

Utilizing our mass proxies, we can establish scaling relations. To understand and calculate the intrinsic scatter, we perform a linear regression using the LINMIX algorithm (Kelly 2007). This code employs a Bayesian approach and considers errors in both parameters, namely masses and proxies, which is particularly suitable for real data. We model the relation as,

$$\log_{10}\left(\frac{M_{200}}{M_\odot}\right) = \alpha + \beta \log_{10}\left(\frac{O}{O_{piv}}\right) \pm \epsilon \quad (1)$$

Here, α and β denote the coefficients, O and O_{piv} stands for the mass proxy and the pivot value equivalent to its mean, and ϵ represents the intrinsic scatter around the regression. The best-fitting parameters resulting from this analysis are detailed in Table,1, where mock values are indicated by "true".

Results are also presented in the Figure 2. The top, middle, and bottom panels illustrate the relationships between Mass and λ, Mass and L_λ, and Mass and $M^\star_\lambda$, respectively. In the figure, black diamonds represent mock results, while red circles represent the estimator outcomes.

Table 1. Best-fitting values from linear regression. Equation,1 describes the mass-observable relation, where O_{piv} is consistently associated with the mock proxy. Optical luminosity (L_λ) and total stellar mass ($M^\star_\lambda$) are presented in units of $L_\odot$ and $M_\odot$ respectively.

Proxy	α	β	ϵ	O_{piv}
λ_{True}	13.85 ± 0.02	1.32 ± 0.07	0.180 ± 0.009	5.4
λ_{AME}	13.86 ± 0.02	0.95 ± 0.10	0.181 ± 0.009	”
$L_{\lambda,True}$	13.89 ± 0.01	0.94 ± 0.05	0.141 ± 0.007	6.7×10^{10}
$L_{\lambda,AME}$	13.89 ± 0.01	0.95 ± 0.05	0.151 ± 0.007	”
$M^\star_{\lambda,True}$	13.92 ± 0.01	1.12 ± 0.04	0.092 ± 0.005	2.4×10^{11}
$M^\star_{\lambda,AME}$	13.99 ± 0.01	1.12 ± 0.03	0.097 ± 0.005	”

Table,1 highlights that the mass-richness relation exhibits the highest scatter. This is not a surprising conclusion as the mock results at the low-mass end emphasize the significant intrinsic scatter for small richness groups. For instance, a structure with $\log_{10}(\lambda) = 0.6$ ($\lambda = 4$) can present a halo mass ranging from $10^{13.2}$ to $10^{14.2}$ M⊙. Despite differences at the high richness end, which indicates some contamination for high mass clusters, the mock and AME linear regressions exhibit consistent behavior. We find an intrinsic scatter of $\sigma\log_{10}(M|\lambda) = 0.181 \pm 0.009$ dex, a value comparable to the one observed in simulations.

L_λ has proven to be a valuable parameter, exhibiting a scatter of $\sigma_{\log_{10}(M|L_\lambda)} = 0.151$ dex, compared to the simulated value of 0.141 dex. Notably, the observed residual scatter between the mock and AME results is consistent with $\sigma_{\log_{10}(\lambda_{True}|\lambda_{AME})}$ which is 0.014.

When considering the amplitude of the mass range, we observe similar behavior for L_λ. However, a slight deviation is noticeable for lower luminous structures, possibly due to external contamination. This difference leads to a minimal increase in intrinsic scatter compared to the simulation.

$M^\star_\lambda$ emerges as a compelling choice with the least intrinsic scatter, offering a robust characterization of galaxy cluster candidates in terms of physical properties like stellar mass. However, these results could be somewhat optimistic as they rely on the precise values obtained from analytical models. In optical surveys, the inference method could introduce scattering or uncertainties. Similar to the pattern observed in L_λ at the low end, we note a minor difference in β, introducing a gap of approximately ~ 0.01.

4.3. Impact of center and redshift variations

To assess the robustness of the code, we introduce slight variations in redshift and center coordinates within the mock cluster catalog. These variations emulate the subtle disturbances encountered in the detection of galaxy clusters using observational data.

In their work, Werner et al. (2022) explore the utilization of the density-based algorithm PZWav (Gonzalez 2014) to identify clusters from S-PLUS DR1. They evaluate the algorithm's performance by comparisons with the detection outputs obtained with the same simulated catalog described in our study. Given PZWav's methodology, which detects structures based on the galaxies' spatial distribution and estimates redshifts considering the surrounding galaxies, observed variations in center and redshifts are small. The average radii offset is 10 kpc, with a scatter of 12 kpc, while for redshifts this difference is as small as 0.6×10^{-3} with $\sigma = 8.8 \times 10^{-3}$.

To examine these variations, we consider three different scenarios involving the mean values added to the 1σ, 2σ, and 3σ intervals. Subsequently, we compare the richness results obtained under these offsets with the centralized ones. The ΔR variations are described as 2D Gaussian distributions, similar to previous studies on miscentering (e.g., Johnston et al. 2007). Importantly, this displacement is not applied over a preferential frame; instead, we randomly draw an orientation value between 0 and 360 degrees.

For Δz, this offset is employed as a normal distribution centered on Δz with corresponding σ_{Norm} values of 1, 2, or 3σ, randomly adding or subtracting from the cluster redshift.

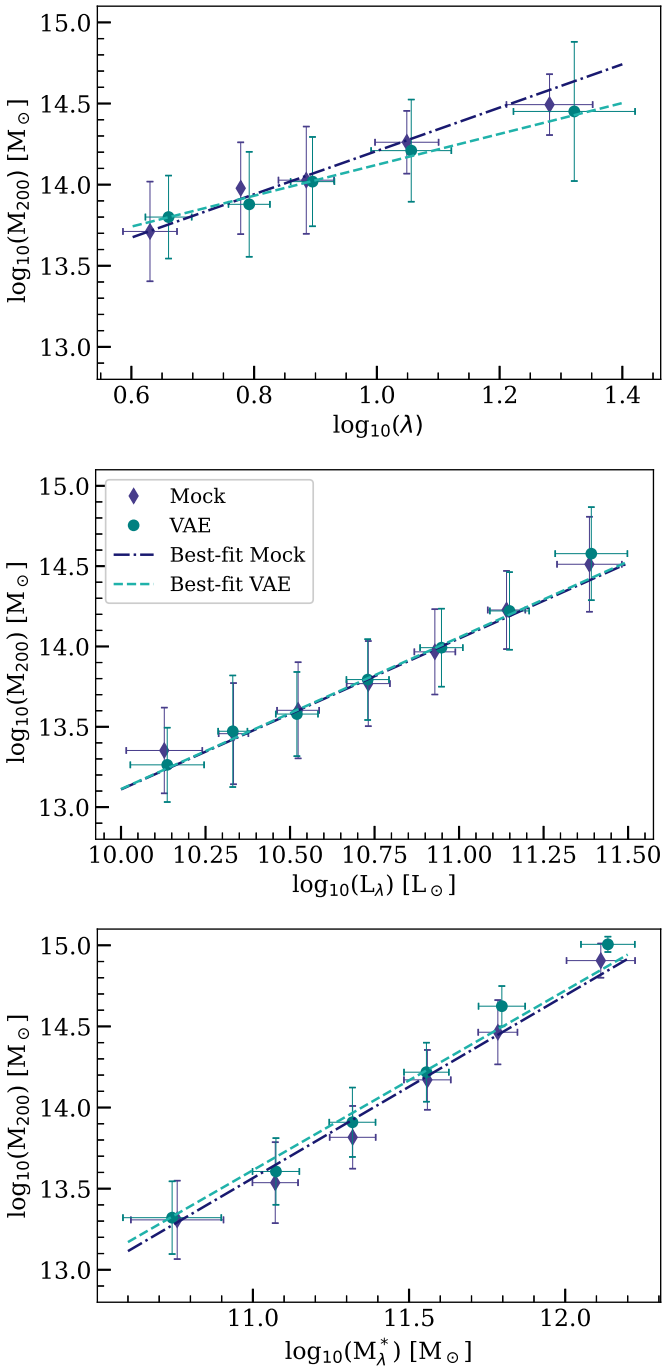

Figure 2. Scaling relations between mass and optical proxies. Median values in proxy bins are highlighted for both the adaptive membership estimator (red dots) and mock values (black diamonds), along with the corresponding linear regressions (orange and grey lines). Coefficient values can be found in Table,1.

Table 2. The median relative error between richness calculated under ΔR and Δz offsets and the centralized ones. These offsets include a mean value added to 1σ, 2σ and 3σ intervals.

	ΔR [kpc]	Δz
$\bar{O} + 1\sigma$	0 ± 0.010	-0.02 ± 0.05
$\bar{O} + 2\sigma$	0 ± 0.011	-0.08 ± 0.10
$\bar{O} + 3\sigma$	0 ± 0.013	-0.18 ± 0.18

Table 2 summarizes our findings. The table includes median relative errors and σ_{MAD} for richness results under variations in ΔR and Δz. As there were no significant trends observed across the redshift range, we consolidated the results for all galaxy clusters within each scenario.

For small offsets in center distance, the richness results exhibit no significant deviation, as indicated by median relative errors consistent with zero. This analysis underscores the robustness of the code against center variations within this range. Upon further investigation, we find that the median relative error remains below -2% even up to $\Delta R > 250$ kpc. However, it increases to -35% for $\Delta R > 500$ kpc and -50% for $\Delta R > 750$ kpc. Here, the negative sign denotes an underestimation of richness. These observations suggest that the code is sensitive to variations in galaxy density at the outskirts of the cluster compared to the central distribution, particularly influenced by the choice of the field galaxies as contamination points.

In the context of redshift variations, we notice a reduction in the richness measurements within the range of error bars. The deviation ranges from -8% for a 2σ offset to -18% for a 3σ offset. This considerable difference, comparable to the photo-z uncertainty, implies the exclusion of a significant contribution from PDFs of galaxies near the cluster center. It's noteworthy that despite these variations, the code demonstrates robustness against expected offsets in both center and redshift.

5. Conclusions

We introduced AME, an adaptive membership estimator (Doubrawa et al. 2023), utilizing photometric redshifts, which provided robust estimates for richness, optical luminosity, and total stellar mass across a dataset of 919 simulated structures. This method minimizes reliance on specific cluster definitions, utilizing only the sky position within a characteristic radius (R_c) to identify potential galaxy members.

Analyses using the true galaxy members, as defined by the simulation, revealed that comparisons between median values of richness estimates with λ_{mock} and λ_{AME} produce a linear relation. The residual value obtained from the individual differences produces a value of -0.01 ± 0.12.

Relying on the membership probabilities, we derive optical mass proxies by weighting galaxy properties according to their memberships. Employing linear regression in the scaling relations between mass and observables, we achieve competitive intrinsic scatter compared to the literature. Specifically, we observe $\sigma_{\log_{10}(M|\lambda)} = 0.181 \pm 0.009$ dex for richness, $\sigma_{\log_{10}(M|L_\lambda)} = 0.151 \pm 0.007$ dex for total optical luminosity, and $\sigma_{\log_{10}(M|M^\star_\lambda)} = 0.097 \pm 0.005$ dex for stellar mass.

We demonstrate the robustness of our adaptive estimator against small center and redshift variations as expected in detection catalogs produced by cluster finders. In the face of these variations, the errors remain below 1%.

Acknowledgements. LD was supported by a scholarship from the Brazilian federal funding agency *Coordenação de Aperfeiçoamento de Pessoal de Nível Superior - Brasil* (CAPES). ESC acknowledges the support of the funding agencies CNPq (#309850/2021-5) and FAPESP (#2023/02709-9). PAAL thanks the support of CNPq (grants 433938/2018-8 and 312460/2021-0) and FAPERJ (grant E-26/200.545/2023). R.A.D. acknowledges partial support from CNPq grant 312565/2022-4.

References

Araya-Araya, P., Vicentin, M. C., Sodré, L., et al. 2021, MNRAS, 504, 5054. doi:10.1093/mnras/stab1133
Bellagamba, F., Sereno, M., Roncarelli, M., et al. 2019, MNRAS, 484, 1598. doi:10.1093/mnras/stz090
Benitez, N., Dupke, R., Moles, M., et al. 2014, arXiv:1403.5237
Campello, R., Moulavi, D. & Sander, J. Density-Based Clustering Based on Hierarchical Density Estimates. *Advances In Knowledge Discovery And Data Mining*. pp. 160-172 (2013)
Castignani, G. & Benoist, C. 2016, A&A, 595, A111. doi:10.1051/0004-6361/201528009
Cenarro, A. J., Moles, M., Cristóbal-Hornillos, D., et al. 2019, A&A, 622, A176. doi:10.1051/0004-6361/201833036
de Jong, J. T. A., Verdoes Kleijn, G. A., Kuijken, K. H., et al. 2013, Experimental Astronomy, 35, 25. doi:10.1007/s10686-012-9306-1
Doubrawa, L., Cypriano, E. S., Finoguenov, A., et al. 2023, MNRAS, 526, 4285. doi:10.1093/mnras/stad3024
Euclid Collaboration, Adam, R., Vannier, M., et al. 2019, A&A, 627, A23. doi:10.1051/0004-6361/201935088
Finoguenov, A., Rykoff, E., Clerc, N., et al. 2020, A&A, 638, A114. doi:10.1051/0004-6361/201937283
Gonzalez A., 2014, in Building the Euclid Cluster Survey - Scientific Program
Henriques, B. M. B., White, S. D. M., Thomas, P. A., et al. 2015, MNRAS, 451, 2663. doi:10.1093/mnras/stv705
Ider Chitham, J., Comparat, J., Finoguenov, A., et al. 2020, MNRAS, 499, 4768. doi:10.1093/mnras/staa3044
Johnston, D. E., Sheldon, E. S., Wechsler, R. H., et al. 2007, arXiv:0709.1159. doi:10.48550/arXiv.0709.1159
Kelly, B. C. 2007, ApJ, 665, 1489. doi:10.1086/519947
Lopes, P. A. A. & Ribeiro, A. L. B. 2020, MNRAS, 493, 3429. doi:10.1093/mnras/staa486
Lopes, P. A. A., de Carvalho, R. R., Kohl-Moreira, J. L., et al. 2009, MNRAS, 399, 2201. doi:10.1111/j.1365-2966.2009.15425.x
Mendes de Oliveira, C., Ribeiro, T., Schoenell, W., et al. 2019, MNRAS, 489, 241. doi:10.1093/mnras/stz1985
Molino, A., Costa-Duarte, M. V., Sampedro, L., et al. 2020, MNRAS, 499, 3884. doi:10.1093/mnras/staa1586
Pacaud, F., Clerc, N., Giles, P. A., et al. 2016, A&A, 592, A2. doi:10.1051/0004-6361/201526891
Pereira, M. E. S., Soares-Santos, M., Makler, M., et al. 2018, MNRAS, 474, 1361. doi:10.1093/mnras/stx2831
Planck Collaboration, Ade, P. A. R., Aghanim, N., et al. 2014, A&A, 571, A16. doi:10.1051/0004-6361/201321591
Pratt, C. T. & Bregman, J. N. 2020, ApJ, 890, 156. doi:10.3847/1538-4357/ab6e6c
Reiprich, T. H. & Böhringer, H. 2002, ApJ, 567, 716. doi:10.1086/338753
Satopaa V., Albrecht J., Irwin D., Raghavan B., 2011, in 2011 31st International Conference on Distributed Computing Systems Workshops, doi:10.1109/ICDCSW.2011.20
Sereno, M., Ettori, S., Eckert, D., et al. 2019, A&A, 632, A54. doi:10.1051/0004-6361/201628521
Springel, V., White, S. D. M., Jenkins, A., et al. 2005, Nature, 435, 629. doi:10.1038/nature03597
The Dark Energy Survey Collaboration 2005, astro-ph/0510346. doi:10.48550/arXiv.astro-ph/0510346
Vikhlinin, A., Kravtsov, A. V., Burenin, R. A., et al. 2009, ApJ, 692, 1060. doi:10.1088/0004-637X/692/2/1060
Weinberg, D. H., Mortonson, M. J., Eisenstein, D. J., et al. 2013, Phys. Rep., 530, 87. doi:10.1016/j.physrep.2013.05.001
Werner, S. V., Cypriano, E. S., Gonzalez, A. H., et al. 2022, MNRAS. doi:10.1093/mnras/stac3273
Willmer, C. N. A. 2018, ApJS, 236, 47. doi:10.3847/1538-4365/aabfdf
Wright, E. L., Eisenhardt, P. R. M., Mainzer, A. K., et al. 2010, AJ, 140, 1868. doi:10.1088/0004-6256/140/6/1868